Applied Innovative Research, ISSN 2581-8198, Vol. 3, Issue 1 - 4, Year 2022

सीएसआईआर- एम्प्री
CSIR-AMPRI

Experimental and Simulation study: Switching in RRAM

Shikha Kaushik[a], Sujata Pandey[a], and Rahul Singhal[b]
[a]*Amity School of Engineering and Technology,*
[a]*Amity University Uttar Pradesh, Noida, India*
[b]*Malviya National Institute of Technology, Jaipur India*

Abstract : The future application of non-volatile memory Resistive Random-Access Memory (ReRAM) has been studied. ReRAM has sparked a lot of interest due to its simple structure, low voltages, fast switching rates, high density packing, and ease of integration into CMOS processing. ReRAM-compatible materials have been proved to be Transition-Metal-Oxides.Because of its fab-friendliness and dielectric constant of 10, ZnO is among the most promising materials among several.A W(electrode)/ZnO/ITO is built and simulated in this study using Multiphysics simulation software. The ReRAMs are designed both with symmetrical and asymmetrical metal connections. The current-voltageand thermal properties of various devices were investigated, as well as the underlying processes. Analysis by AFM, SEM, and RBS was also done. During the ON state, it really is noticed that metals with low thermal conductivity lose less heat thus creating high temperatures.Excellent switching performance is achieved in W(electrode)/ZnO/ITO device measured by pressure contact. A resistance ratio of $1.3x10^5$ was also obtained, proving the device's resiliency with exceptional memory window performance. As a result, the systems are developed and compared to the simulated devices.

Keywords: ReRAMs; memory window; switching; sputtering; thin film

Introduction

Over the last decade, the memory hierarchy of computers have evolved to incorporate NAND flash-based memory with DRAM. Because these memories can only be scaled so far, new technologies are required. One trend is the development of novel ReRAM material with three-dimensional structures that display an excellent resistive switching phenomenon. The fundamental advantage of ReRAM technology is that this is compatible with CMOS technologies. The scaling merit works in terms of both the ReRAM process's low power consumption. Due to its scalability & operating speed limit, ReRAM appears positioned could replace standard flash memory technology devices, particularly for memory applications needing quick operation with medium storage density [1-2]. ReRAM's capabilities aren't restricted to flash memory replacements. This development of next-generation compact memory devices featuring improved performance was required in futuristic data storage [3-4]. ReRAM, which features a higher write/read speed as well as a lower programming voltage, seems to have the potential to replace Flash memory. ReRAM offers a number of benefits over other developing memory alternatives, including ease of manufacture, extended data retention, a simple structure, nanosecond velocity, exceptional scalability, & compatibility using current CMOS technology, making it a potential option for future digital memory [5].Various metals oxides have indeed been tested on a range of materials in recent years. Impedance switching of non-volatile metal oxide-based materials like (HfOx) hafnium oxide[6], (TiOx) titanium oxide [7], (TaOx) tantalum oxide [8], (NiO) nickel oxide [9], (ZnO) zinc oxide [10], (MnOx) manganese oxide [11], (MgO) magnesium oxide [12], (AlOx) aluminium oxide [13], and (ZrO_2) zirconium dioxide [14] has sparked the most attention but been extensively researched in recent years. TiOx and Zinc oxide (k=10) are two of its most promising materials amongst them because of their fab-friendly, increased dielectric constant (k=80) [15-17]. Because oxygen vacancies are generated, ion irradiation is beneficial to enhance ReRAM properties[18]. A variety of materials were used to create ReRAM electrodes[19].ReRAM seems to be a two-terminal device made up of two electrodes and a 10-140nm thick insulating layer. An electrical channel could be constructed thru the oxide insulator withinthe form of something like a conductive filament. The ON state of a system produced during the SET and then ended during the RESET is represented by the more can filament regime. Heat flows as a result of the high current flowing through a filament, resulting in a temperature distribution which impacts the system's operation.Therefore, in the paper,the layer of Zinc

** Corresponding author:(E-mail: rsinghal.phy@mnit.ac.in)*

oxide was deposited over such an ITO-coated glass, and after that electrical transport would be conducted with the help of pressure contact using a Keithley instrument, and an excellent switching behaviour with just a ratio of both the order of 5 would be measured, that is very useful for RRAM applications [20]by constructing the identical device using COMSOL programme and doing the I-V appropriately. Asymmetrical and symmetrical devices were modelled and evaluated for I-V characteristics and temperature distribution during the ON/OFF state to produce an optimal construction. For both the constructed and simulated devices, I-V factors have been found. As during ON state, it's also noticed that metals with low thermal conductivity lose less heat and create high temperatures. RBS, SEM, and AFM techniques were used to evaluate crystallinity, content, surface morphology, etc thickness.

Device Physics and Working Principle

Resistive switching is often used to operate it. Electro-structural transitions play a role in the formation as well as a breakdown of either the conductive filament as well as the oxide layer beneath the electric fields, resulting in the formation of two states: a low resistance state (LRS) as well a high resistance state (HRS), which seem to be comparable to '1' and '0' states.Binary metal oxide-based ReRAM materials have been shown to be CMOS compatible or could be easily coupled using advanced node CMOS technology with BEOL [21]. According to the design and switching polarity, ReRAM devices are classed as unipolar or bipolar.As shown in Fig.1a, the forward and reverse voltage could be used to construct and reset unipolar ReRAMs. These systems' switching characteristics aren't any longer polarity dependent. Primarily to avoid excessive heat generation, which could cause the conductive filament to be exterminated right following synthesis, only related devices could utilise the current enforcement during the set. During reset, however, a significant current was purposefully created to break the conductive path, forcing its system to revert towards the (HRS)high resistance state [22-23]. Whenever a positive voltage was provided all throughout the system with bipolar ReRAMs, only the stable configuration shown in Fig.1b remains possible. Aside from just that, every reset phase requires a voltage that is still the polar opposite of that utilized during the set phase. The device seems to be a bipolar ReRAM if indeed the voltage is negative. Bipolar devices seem to be more energy-efficientefficient than unipolar transistors and have lower reset currents [24]. The electrode materials as well as the symmetry of something like the device structure dictate polarity in ReRAM devices asgiven in Table 1.

Table 1: Several kinds of oxides&electrodes, as well as their related switching modes, were depicted.

Unipolar	**Bipolar**
Pt/Al_2O_3/Pt [2]	Ti /Al_2O_3/Pt [1]
Pt/CoO, NiO /Pt [3]	Pt, Ta/ CoO /Pt1Ta [4]
Ni, CO/Cu_2O/Cu [6]	Al, Pt, Ti /CuXO/Cu [7]

The switching context of information systems with the formation/rupture of metal-ion-rich conductive filaments is divided into three major operations: formation, reset and set. Pristine electronics may well have high resistance values but will need to be initiated until powerful resistive switching mechanisms might well be realized. The ReRAM unit would be in the LRS once the conductive filament was formed, as well as the topelectrode and bottom electrode were linked by a conducting filament.The current compliance imposed through Set/Forming operations determines the Low Resistance State value. And during the forming process, larger voltages were required than in normal resistive switching settings [25-31]. The electrical filament partially melts after being reset, and the ReRAM system returns to its HRS. Thermal breakdown of something like the conductive filament, including electrode/oxide interface characteristics that can affect atomic behaviour throughout ReRAM operations has all been investigated in order to truly comprehend its reset process [32-33]. It's comparable to a forming process, however, a lower applied voltage seems required to restore its conductive filament that has been broken during reset operation. Following the set operation, the ReRAM was set to LRS and can be switched among its two states numerous times (HRS and LRS). The memory window is presented as a factor of HRS/LRS.

Device physics of ReRAMs:

ReRAMs were categorised in several ways based on the operating ideas and applied physics. Electrochemical Metallization (ECM) ReRAMs and oxygen vacancies are both affected by oxygen vacancies (OV-based) Therefore in sense, these two main kinds of storing devices are ReRAMs and DRAMs.

In ECM ReRAMs, a metallic conductive filament arises because the metal cation seems to have a greater diffusivity than that of the oxygen anion. In OV-based ReRAM, oxygen anions were substantially more diffusive than metal cations, and hence play a significant influence in system characteristics. In oxygen vacancies-based ReRAM, a conductive filament in an on is caused either by traps generated more by oxygen vacancies. Some physical processes that influence the switching mechanism of ReRAMs are described in this report.The oxygen ions would wander from where they have been previously based on the positive voltage given to the top electrode.The top and bottom electrodes are connected via the functional layer even by the resultant conductive filament pathway.The oxygen vacancies withinthe filament increase the electrical conductivity of the resistive thin film and also change the MIM from HRS to LRS. Whenever an electrode becomes subjected to either a negative voltage, the oxygen ions migrate back toward the resistive switching layer, causing the created conducting filament would rupture, and the MIM to return to HRS [32]. Duringthe development & destruction stages of something like the conduction filament, oxygen vacancies & oxygen ions are the most prominent features of the functional layer. The oxygen vacancies of OV-based ReRAMs play an important role in the development of both the conducting filament. In those kinds of systems, oxygen vacancies tend to become more variable than metal cations. As a result, the system's oxygen vacancy concentration with resistance has an inverse relationship. It is necessary to understand whether oxygen vacancies impact device conductivity as well as how the concentration of oxygen vacancies may be changed through voltage application [33-35]. As a result, the electron concentration grows as even the oxygen vacancy concentration rises. Oxygen vacancies are commonly used as charge traps in broad bandgap materials like HfO_2 and ZrO_2 [36]. With symmetrical connections, they offer an overview of something like the temperature distribution (both top and bottom contacts are the same metal), and asymmetrical metal connections (top and bottom contacts have distinct metals), with an emphasis on that underlying physics to improve the system's knowledge and design. This investigation is conducted out numerically by producing temperature distributions under various conditions.

Experimental and characterization:

Indium tin oxide (ITO) glass was split into several 1x1cm2 samples for thin film deposition. The glass sample was washed using a solvent prior to ZnO deposition. The samples were loaded into the sputtering chamber, which could pump down to 7.6x10-6 mbar before deposition. Using an RF gun with such a deposition rate of 0.3-0.4Å/s as well as a continuous Ar gas flow, a thin coating ZnO was deposited on an ITO covered glass substrate. The chamber pressure remained 8.2×10^{-3} mbar, as it has been since deposition. The RRAM concept is shown in Figure 1.

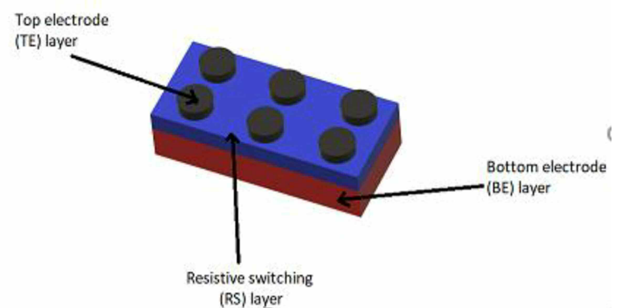

Figure 1: Schematic of ReRAM

Thin-filmCharacterization:

On an ITO coated Glass, ZnO thin films are deposited as stated above. To explore the thickness & chemical content of both the thin coating, RBS was performed using 2 MeV alpha particles from a 1.7 MV tandem Pelletron accelerator. A compositional study was performed using peak-fitting software. But using an NSG 30, atomic force microscopy (AFM) is utilised to examine the surface roughness there in the AC mode tip (non-contacting mode) area. The surface roughness was analysed with Gwyddion software, and also the watershed approach was utilised to obtain cluster radius. A Nova Nano FE-SEM 450 (FEI) device.The morphological features of both the particles were investigated using this method. Scanning electron microscopy was used to characterise the pristine (as deposited) (SEM). The nanoparticle size distribution was examined using ImageJ®software.

They utilised a two-probe probe station with a Keithley 6517b electrometer and a pressure contact constructed of W metal to get I-V characteristics.

To really get the I-V characteristics, the voltage there at top electrode were swept from -2 to +2V.

Experimental and Characterization Results:

Atomic force microscopy had been used to investigate the surface morphology of ZnO films. The topographic images of a virgin are shown in the figure. The closely packed particles with a consistent size

distribution were clearly apparent in topographic images with as-deposited films. The particles' borders were similarly well defined. The average size of ZnO film is 19±2 nm.

"The layer has a roughness of 35 nm when that is produced. As is seen in Fig 2, the thin film of ZnO generated through this basic RF sputtering technique has an exceptionally smooth surface shape.

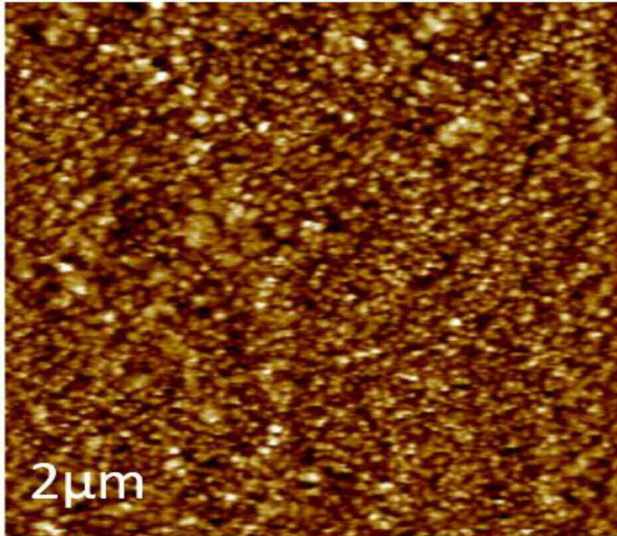

Figure. 2 AFM

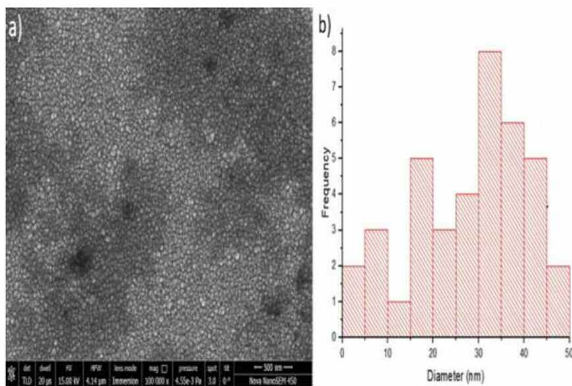

Fig.3(a) SEM images showing nanoparticlesizeand 3 (b) histogram of ZnO-ITO surfaces

The nanoparticle size dispersion of deposited films is 16–50 nm in SEM. Figure 3 shows SEM images of ZnO-ITO surfaces with respect to respective nanoparticle size distribution (a).

The surface morphology creates lumps of micro and nano hierarchical structures that are equally dispersed.

Furthermore, as can be seen in Fig 3, the size distribution changes among granular sizes of 10nm and 50nm (b). RBS measurements were performed on ZnO thin films on ITO-coated glass. Figure 4 illustrates the RBS spectrum of a ZnO thin layer on glass using ITO.

The SIMNRA simulation is being used to match the spectra to calculate the thickness of the coating and zinc, oxygen atomic percentage.

According to here on SIMNRA simulation with such a layer thickness of (138±10) nm, the zinc atomic fractions were determined to be 55.0 per cent of oxygen and 45.0 per cent, respectively. Indium has a 45 per cent atomic fraction, tin has a.05 per cent atomic fraction, while oxygen has a 50 per cent atomic fraction.

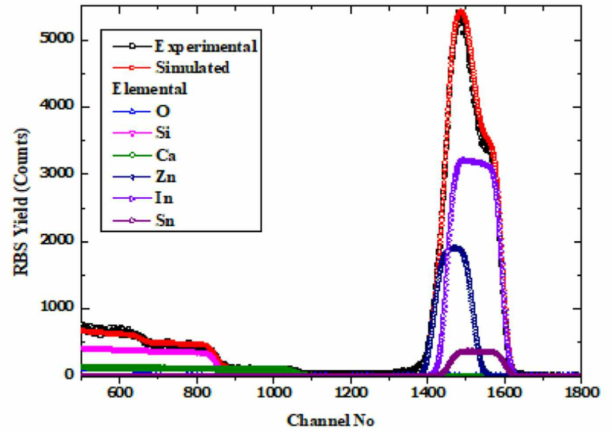

Figure. 4 RBS spectra

Electrical characteristics:Table 2 shows that by employing pressure contact, as demonstrated in my previously reported work [20], we were able to achieve an outstanding ratio of the order of 5.

S.NO	MATERIAL	RATIO	REF
1.	Pt/ZnO/Pt	10^3 - 10^4	37
2	Pt/ZnO/Ag0.2-Al0.8/A	$>10^2$	38
3	Pt/ZnO/Cr/ZnO/Pt	10^4	39
4	AZO/ZnO/ITO	14	40
5	TiN/ZnO/Pt	10	41
6	Ag/ZnO/Cu	10^3	42
7	Al/ZnO/Al	10^4	43
8	W (electrode)/ZnO/ITO Pressure contact	10^5	20 (our previously reported work)

Table 2: Comparison of resistance ratio by using zinc oxide

Simulation Model: An insulating layer,an insulating layer, as well as a metallic filament make up the ReRAM simulation model shape. The thickness of the electrodes, which are 30 nanometers thick, varies with different metals used in the simulation. Our active

substance, which really is 100 nm thick, seems to be the insulating layer. A filament is a switching component that they introduce. We use this filament to add switching behaviour towards the active material. Figure 6 shows the device schematic.

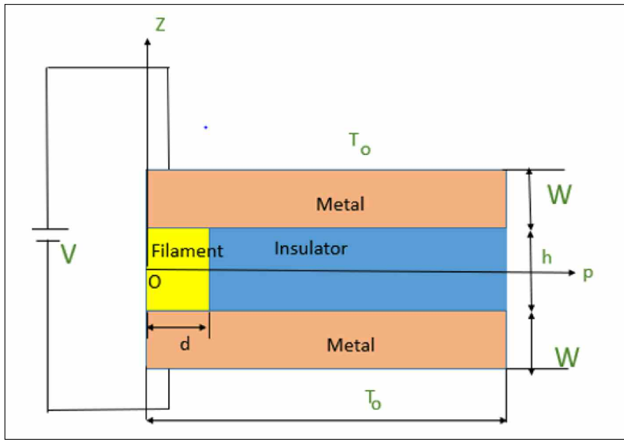

Figure 5: A simulation model of ReRAM. W shows the thickness of the metal electrodes, h is the thickness of the filament, d is the radius of the filament, and T0 represented the initial temperatures of the respective electrodes.

Table 3 lists the model parameters for such active layer and filament that were utilised there in simulation.

Metal	ZnO	Model A Filament (ON state)	Model B Filament (OFF state)
Thermal conductivity[W/K.m]	50	50	40
Electrical Conductivity[S/M]	7.21E-7	2E3	3E-3
Specific Heat [J/kg.K]	40.3	40.3	38.3
Relative Permittivity	8.5	8.5	6.5
Density[kg/m3]	5660	5660	5660

Table 3: Presumed value between Zinc and Zinc Oxide (For Material Switch)

The parameters researchers utilise to simulate the active layer are represented in the first column (ZnO). The ON (LR State) and (OFF) HR State is represented more by the second and third columns, respectively. They have two options for modelling the metal connections. For starters, they may use asimilar metal for top and bottom electrodes, which itself is known assymmetric metal contact. Second, two dissimilar metals could be used to represent either top and bottom electrodes, which is known as an asymmetric metal contact. They use the following electrode materials to create symmetric and asymmetric metal contact situations – ITO, AuTiN, Hf, W, Al, Au, Cu, Ag. Table 4 lists the parameters of the electrode materials employed in the simulation model. Its top electrode's voltage is linked to a variable V0, whereas the bottom electrode remains grounded. These electrical simulations were carried out using the COMSOL Multiphysics simulation program.

Metal	ITO	TiN	Hf	W	Al	Au	Cu	Ag
Thermal conductivity[W/K.m]	10.5	11.9	23	175	247	310	398	429
Electrical Conductivity[S/M]	106	106	3.106	106	3.5x107	4.5x107	5.9x107	6.3x107
Specific Heat [J/kg.K]	135	545.33	144	132	887	130	385	236
Relative Permittivity	-1E6	-1E6	-1E6	-1E6	-1E6	-1E6	-1E6	-1E6
Density[kg/m3]	0.00714	5220	13310	17800	2700	19300	8940	10497

Table 4: Material parameters of various metals were used in this simulation. [36–38]

Multiphysics used in simulation: The ReRAM devices are simulated using two physics but one Multiphysics module. The heat transport in solids and electric current are some of the physics modules. Researchers also employ electromagnetic heating to represent the effect of heating within those ReRAM devices as a result of the current flowing through them. Module for Multiphysics.

Several governing equations, which include the Fourier law continuity equation as well as the current conservation law, were presented below. Every one of the simulations were done in a steady state environment.

To get electromagnetic heating from the inside of the structure, electric current and heat equations were solved and connected. Heat transfer in solids is offered as a solution like this in all domains:

$$\rho Cp\cdot u\, T + \cdot q = Q + Qted$$

Qted indicates the thermoelastic impacts, Where U is the velocity, Cp is the specific heat capacity, ρ is the density, Q is the heat source, while ∇T represents a temperature gradient, q represents heat flow, and k represents thermal conductivity. For heat conduction, this is recognized also as Fourier law. The equation for

thermal continuity seems to be as follows,

$$q = -k\nabla T \quad (2)$$

This structure's right margins were thermally insulated. They retain several of the structure's terminals at 300K for first boundary conditions.

Consequently, the right edges of the structure were electrically insulated by electric current, thus current was preserved. The continuity equation, which itself is given as, then solved in each of the components:

$$\nabla \cdot J = Q \quad (3)$$

When inserting an externally produced current J, this current density relation becomes generalised. The constitutive relationship that results is:

$$J = \sigma E + J \quad (4)$$

$$E = -\nabla V \quad (5)$$

where J represents current density, V represents potential, the electric field in the filament is represented by E and σ represents electrical conductivity. V0 Voltage was changed, while the other terminal remained grounded.

Electromagnetic heating is caused by the interaction of heat transfer & electric current. These equations that control the phenomena are just as follows:

$$\rho Cp \cdot \nabla T = \nabla \cdot (k\nabla T) + Qe \quad (6)$$

$$Qe = J \cdot E \quad (7)$$

Results and discussion

A non-uniform mesh and indeed the necessary physics was developed just after the structure was formed. For such ReRAM devices, the associated heat and electrostatic equations are solved numerically. they'll look at just how metal connections impact temperature distribution in ReRAM devices in just this section. Various metal contacts have distinct thermal conductivities, resulting in different temperature gradients within ReRAM. To begin, we'll look at the example of symmetrical interactions. Both top and bottom electrodes are the same in this situation. Figure 6 shows the temperature gradient for the symmetric device.

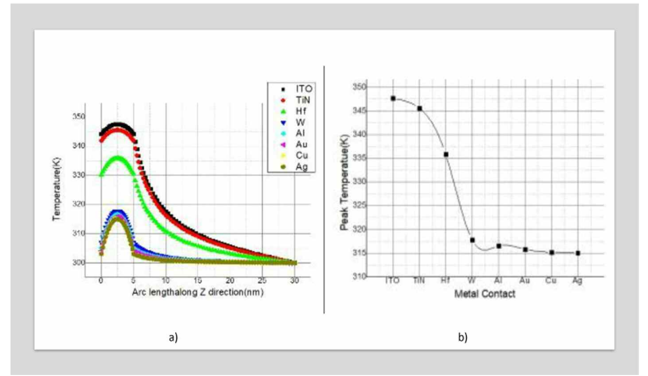

Figure 6: (a) shows the temperature gradient is symmetrical and identical in the symmetrical contacts in z directing (b) Shows a graph between peak temperature and symmetrical metal contacts in z (axial) directing

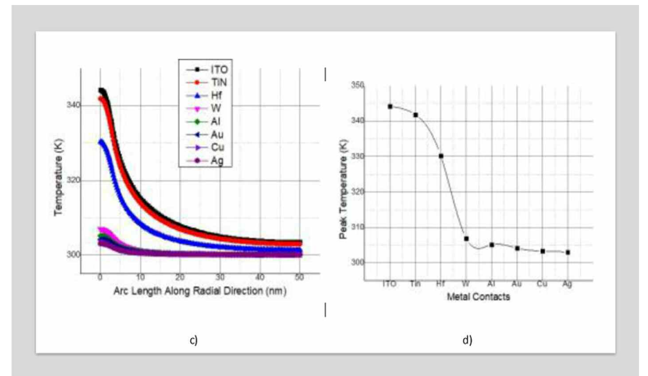

Figure 6 (c) Shows the temperature gradient in the radial direction using symmetrical metal contacts(d) shows the graph between the peak temperature gradient and symmetrical metal contacts in the radial direction.

As seen in Fig. 6 and Table 4, metals with low thermal conductivity lose less heat, heat up quickly, and retain greater heat. As a result, the gadgets' internal temperatures rise.

Across all circumstances, the maximum temperature is found in the switching filament near the device's centre. In the path outwards first, from the filament, overall temperature decreases both in the axial and radial directions.

As shown in Fig.6, the peak temperature was highest in ITO and lowest in Ag, which corresponds to the respective varied thermal conductivities. The peak temperatures retrieved at 2.5 V along the axial and radial axes are shown in Figs. 6(b) and 6(d).

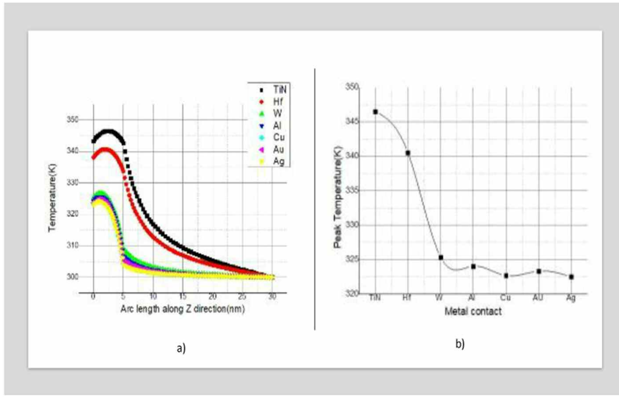

Figure 7 :(a) shows a non-uniform temperature gradient in the asymmetrical metal contacts along z (axial)-direction (b) shows the metal having higher thermal conductivity having lower temperature as it dissipates more heat along z(axial)-direction

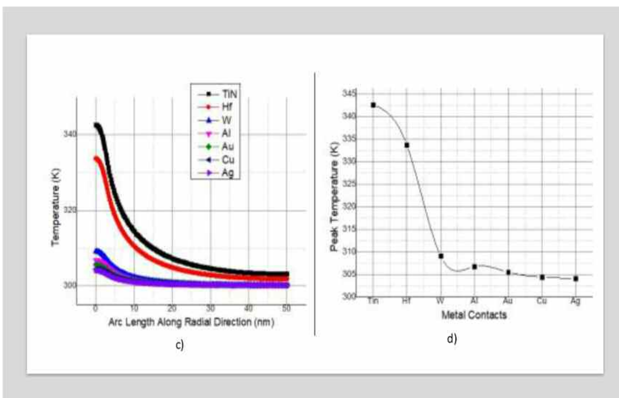

Figure 7 (c) shows a non-uniform temperature gradient in the asymmetrical metal contacts along the radial direction (d) shows the metal having higher thermal conductivity having lower temperature as it dissipates more heat along the radial direction."

The curves with each device withina radial direction are shown in Fig.7. Inside this model, the bottom electrode was maintained constant while the top electrode is changed. All of the instances have a radial direction that ranges from 0 to 30 nm. Contact with such a low thermal conductivity would dissipate less heat and thus retain more heat, resulting in higher temperatures. Temperatures are always highest at the filament in the centre of the device. As per Fig. 7, the metal with just a lower temperature and a rapid drop in temperature as it moves away first from the filament is desirable for ReRAM operation. Metal contact with the high temperature inside the filament as well as a slowly dropping temperature because it drifts away first from the filament, on the other hand, could induce overheating and raise reliability problems. Especially compared to TiN and Hf, Ag, Cu, or Au contacts are particularly good even though they all feature strong thermal conductivities. Whenever researchers employ symmetrical metal connections (Ag on both the top and bottom electrodes), the temperature distribution on both sides of both the insulator material should be symmetrical as well. Figure 8 shows this phenomenon (a).In the case of asymmetrical metal contacts (Ag was also used as the top electrode in this example), while ITO is being utilized as that of the bottom electrode), the thermal conductivities of two metals may differ, based on a non-temperature distribution from around the insulator. Metal contacts with higher thermal conductivities dissipate heat faster than metal contacts with lower thermal conductivities, and vice versa. That phenomenon may be seen in 8 (b).

Figure 8: (a) Symmetrical Contours

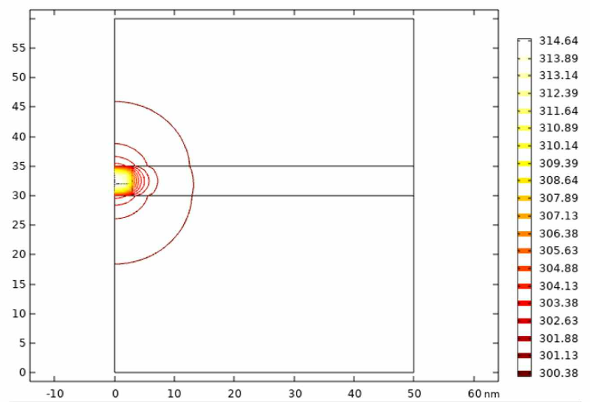

Figure 8 (b) Asymmetrical Contours

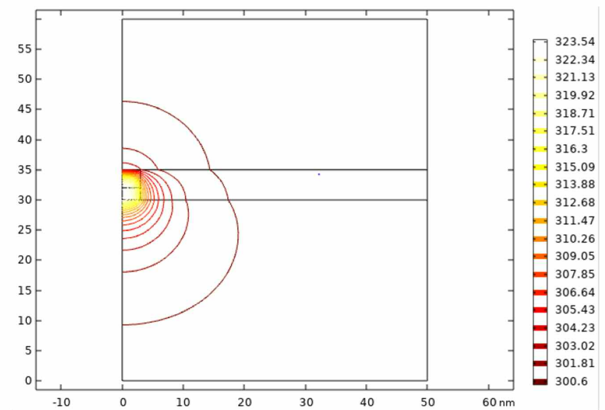

Model validation with experimental results:

Researchers fit our experimental data towards the COMSOL model to verify the model. One is for the ON state, while another is for the Off state. Figure 9 depicts the fitted IV characteristics (b). Table 3 shows the model parameters that were utilised to perform this experiment. Figure 9 (a) depicts a schematic from both models. The metal connections & insulator layer on Model A and B are identical. The filament is indeed the distance between both.

They have the filament turned on in model A, this belongs to the system being in a low-resistance condition (LRS). The filament with model B is represented by values from the OFF state, as indicated in Table 3, whichbelongs to the system being in the OFF state high resistance state (HRS).

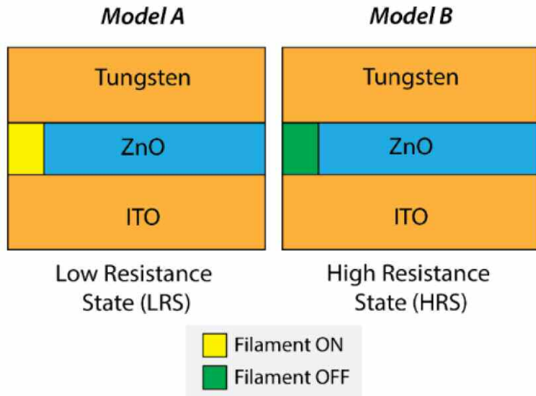

Figure 9 (a): Schematics for Model A & Model B

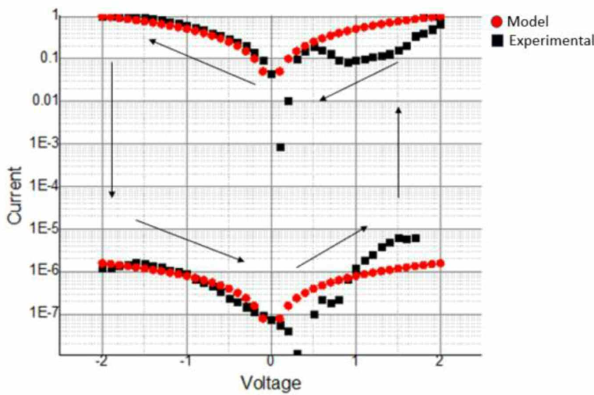

Figure 9 (b): I-V of Simulation &Experimental

In both models [44-45], researchers maintained many of the physical attributes of all layers save the filament the same. To best suit, the data, only the electrical conductivity of both the filament is changed in models A and B. As can see from Table 3 that the filament seems to have greater electrical conductivity than just the insulator layer, even when it is turned off (ZnO). The gadget has no conductive filaments in its original condition. When a voltage is applied to ZnO, conductive filaments emerge which have orders of magnitude more electrical conductivity than pristine ZnO. In models A and B, they model something as a lumped filament.The electrical conductivity of both the conductive filament decreases so when voltage is reversed, even though it is no longer the same as pure ZnO. According to our model, the electrical conductivity of the conductive filaments there in HRS is six orders lower than those in the LRS. Considering that, the HRS filament has a conductance of three orders of magnitude greater than clean ZnO. Although all the other model parameters stay constant, one may deduce that after the filaments are created, the electrical characteristics change from pristine ZnO. Fig. 9 (b)shows the experimental data and our model fit. Non-ideal behaviours such as electron traps, whose wasn't included in the model because of simplicity, might explain the differences here between the model as well as the experiment.

Conclusion

W(electrode)/ZnO/ITO ReRAM is built & simulated with Multiphysics simulation software in this study. The thermal and electrical characterisation of ZnO-based ReRAM is the subject of this research. So that such an optimum structure may be developed, either symmetrical or asymmetrical devices are modelled and evaluated for I-V characteristics and temperature distribution during in the ON/OFF state. For both constructed and simulated devices, I-V factors have been found. At 2V, the resistance ratio here between HRS and LRS states is 105. In addition, they describe the temperature distribution using symmetrical & asymmetrical metal contacts, with only an emphasis on physics to improve the design & comprehension of both the system's physics.AFM additionally revealed the presence of a uniform layer of Zinc oxide." Eventually, actual manufactured and simulated device results are compared and found to be in good agreement.

Acknowledgement

"The authors gratefully recognise the Department of Science and Technology, Government of India, for financial assistance underneath the Women Scientist Scheme (reference number SR/WOSA /ET-91/2018). They gratefully Acknowledge G.R. Umapathy, IUAC, Delhi, for the RBS measurements."

References

[1] R Waser, M Aono Nanoscience and Technology: A Collection of Reviews from Nature Journals, (2010)158–65.

[2]. CY Lin, PH Chen, TC Chang, WC Huang, YF Tan, YH Lin, WC Chen, CC Lin, YF Chang, YC Chen, HC Huang. Materials Today Physics, 13 (2020) 100201.

[3] D. Ielmini, Semiconductor Science and Technology, 31 (2016) 063002.

[4] K. Terabe T. Hasegawa T. Nakayama and M. Aono. Nature,433 (2005) 47–50.

[5] X. Yang, Journal of Nanoscience, (2016).

[6] A. Fantini , D.J. Wouters, R. Degraeve, L. Goux, L. Pantisano, , G. Kar, Y.Y. Chen,, , B. Govoreanu, J.A. Kittl,, , L Altimime. and M. Jurczak, In 4th IEEE International Memory Workshop, (2012) 1–4. IEEE.

[7] H. Ryu, S. Kim. Metals, 11 (2021) 1199.

[8] A. Prakash, D. Deleruyelle, J. Song, M. Bocquet, H. Hwang, Applied Physics Letters, 106 (2015) 233104.

[9] G. Ma, X. Tang, H. Zhang, Z. Zhong, J. Li, H. Su, Microelectronic Engineering,139 (2015) 43–7.

[10] Wu, S. Jian, F. Wang, Z. Chao Zhang, Y. Li, Y.M Han, Z. C Yang, J. S Zhao, and K. L Zhang, Chinese Physics B, 27 (2018) 087701.

[11] H. Abbas, A. Ali, J. Jung, Q. Hu, M. Park, H. Lee and C. J. Kang, Applied Physics Letters, 114 (2019) 093503.

[12] T. Zhang, J. Yin, Y. Xia, W. Zhang, Z. Liu, Journal of Applied Physics, 114 (2013)134301

[13] W. Banerjee, X. Xu, H. Liu, H. Lv, Q. Liu, H. Sun, S. Long, M. Liu, IEEE Electron Device Letters, 36 (2015) 333–5.

[14] M.C. Wu, WY. Jang, CH. Lin, TY. Tseng, Semiconductor Science and Technology, 27 (2012) 065010.

[15] J. J. Yang, M.D. Pickett, X. Li, D. A. Ohlberg, D.R. Stewart, R. S. Williams, Nature nanotechnology, 3 (2008) 429–33.

[16] D. Jana, S. Samanta, S. Roy, Y.F. Lin, S. Maikap, Nano-micro letters, 7 (2015) 392–9.

[17] A. Barman, C.P. Saini, P.K. Sarkar, G. Bhattacharjee, G. Bhattacharya, S. Srivastava, B. Satpati, D. Kanjilal, S.K. Ghosh, S. Dhar, A. Kanjilal, Journal of Physics D: Applied Physics, 51 (2018) 065306.

[18] K.C. Chang, T. Dai, L. Li, X. Lin, S. Zhang, Y.C. Lai, H.J. Liu, Y. E. Syu, Nanoscale. 1243 (2020) 22070–4.

[19] U. Russo, D. Ielmini, C. Cagli, A.L. Lacaita, IEEE Transactions on Electron Devices, 56 (2009) 186–92

[20] H.S. Wong, H.Y. Lee, S. Yu, Y.S. Chen, Y. Wu, P. S. Chen, B. Lee, F.T. Chen, M.J. Tsai. Proceedings of the IEEE.100 (2012) 1951–70.

[21] S. Kaushik R. Singhal, D. K. Avasthi. In2020 IEEE International Conference on Electrical Engineering and Photonics (EExPolytech) (2020) 22–25. IEEE

[22] S. Kaushik, S. Pandey and R. Singhal. ECS Journal of Solid-State Science and Technology (2022).

[23] M. Alayan. Investigation of HfO2 based Resistive Random-Access Memory (RRAM): characterization and modeling of cell reliability and novel access device (Doctoral dissertation, Université Grenoble Alpes).

[24] S.E. Ahn, B.S. Kang, K.H. Kim, M. J. Lee, C. B. Lee, G. Stefanovich, CJ Kim, Y. Park. IEEE electron device letters, 30 (2009) 550–2.

[25] G.M. More, A.P. Tiwari, K.D. Pawar, T.D. Dongale, T. G. Kim. In Mem-elements for Neuromorphic Circuits with Artificial Intelligence Applications, (2021) 299–323.

[26] T.N. Fang, S. Kaza, S. Haddad, A. Chen, YC. Wu, Z. Lan, S. Avanzino, D. Liao, C. Gopalan, S. Choi, S.Mahdavi International Electron Devices Meeting (2006) 1–4. IEEE.

[27] F. Zahoor, T. Z. Zulkifli, F. A. Khanday, Nanoscale research letters, 15 (2020) 1–26.

[28] H. Akinaga, H. Shima, Proceedings of the IEEE, 98 (2010) 2237–51.

[29] C. Lammie, M.R Azghadi, D. Ielmini. Semiconductor Science and Technology, 36 (2021) 065003.

[30] W.C. Chien, Chen Y.R. Chien, Y.C. Chen, A.T. Chuang, F.M. Lee, Y.Y. Lin, E.K. Lai, Y.H. Shih, K.Y. Hsieh, C.Y. Lu, IEEE International Electron Devices Meeting (2010) 19–2.

[31] Z. Shen, C. Zhao, Y. Qi, W. Xu, Y. Liu, I. Z. Mitrovic, L. Yang, C. Zhaom, Nanomaterials, 10 (2020)1437.

[32] U.B. Isyaku, M.H. Khir, I.M. Nawi, M.A. Zakariya, F. Zahoor. IEEE Access (2021).

[33] S. H. Jo, Materials and Devices, Semicon Korea.138 (2015).

[34] CA Betty, S. Choudhury. Sensors and Actuators B:

Chemical 237 (2016)787–94.

[35] G. G. Marmitt Metal oxides of resistive memories investigated by electron and ion backscattering. Thesis (2017).

[36] W. Y. Chang, Y.C. Lai, T.B. Wu, S.F. Wang, F. Chen, M.J, Applied Physics Letters, 92 (2008) 022110.

[37] Z.Q Wang, H.Y Xu, L. Zhang, X.H Li, J.G Ma, X.T Zhang, Y.C Liu, Nanoscale, 10 (2013) 4490–4.

[38] L.C Chang, H.L Kao, K.H. Liu. Journal of Vacuum Science & Technology A: Vacuum, Surfaces, and Films. 32 (2014) 02B119.

[39] F.M. Simanjuntak, D. Panda, T.L. Tsai, C.A. Lin, K.H. Wei, T.Y. Tseng. Journal of materials science, 50 (2015) 6961–9.

[40] N. Xu, L.F. Liu, X. Sun, C. Chen, Y. Wang, D. D. Han, X.Y Liu, RQ Han, J. F Kang, B. Yu, 23(2008) 075019

[41] N. M. Muhammad, N. Duraisamy, K. Rahman, H. W. Dang, J. Jo, K.H. Choi. Current Applied Physics, 13 (2013) 90–6.

[42] C.L Lin, C.C Tang, S.C Wu, P.C Juan, T.K. Kang Microelectronic Engineering. 136 (2015)15–21.

[43] S.K. Deshmukh Nanoscale Electrical and Thermal Interfaces to Resistive Memory Devices. Stanford University; 2020.

[44] C. Lammie, M.R. Azghadi, D. Ielmini. Semiconductor Science and Technology, 36 (2021) 065003.

[45] D. Niraula, V. G. Karpov. IEEE Transactions on Electron Devices. 64 (2017)4106–13.